A DETAILED ANALYSIS OF AN EARTH-MARS LASER TRANSPONDER LINK

John J. Degnan
Geoscience Technology Office, Code 920.3
Laboratory for Terrestrial Physics
NASA Goddard Space Flight Center
Greenbelt, MD 20771 USA

1. INTRODUCTION

Although modern SLR systems are capable of sub-cm ranging accuracies and 50 picosecond time transfer between remote clocks over typical near-Earth satellite distances [Degnan, 1993], extending these unique capabilities to the inner planets and beyond requires that we adopt a new approach. To overcome the prohibitively large R^{-4} signal loss characteristic of single-ended links to passive reflectors, we must utilize two-way laser links, which we refer to generically as "transponders". In such systems, which have a transmitter and ranging receiver at both terminals, the signal strength at each terminal falls off only as R^{-2}. The feasibility of interplanetary laser transponders was introduced in the Proceedings of the last two International Workshops on Laser Ranging [Degnan, 1996; Degnan et al, 1998]. A detailed theoretical treatment, which includes relevant noise models, has recently been submitted for publication [Degnan, 2000a]. The present paper seeks to provide an overview of the theoretical results as well as a detailed analysis of some potential near-term Earth -Mars transponder links. In particular, we look at two alternatives which makes use of existing engineering capabilities within NASA: (1) a MOBLAS ranging to a MOLA-sized (MOLA = Mars Orbiter Laser Altimeter) instrument on the surface of Mars at a 5 Hz rate; and (2) the photon-counting SLR2000 system ranging to a MLA- sized (MLA = Messenger Laser Altimeter) instrument at a 2 kHz rate.

The use of microwave or laser transponders had previously been proposed for lunar ranging [Bender et al, 1990]. Laser transponders on the Moon would make lunar ranging accessible to the smallest of the global SLR stations, and the resulting orders-of-magnitude higher signal strengths would remove the current tracking limitations near "New" and "Full" Moon. The NASA Goddard Space Flight Center is presently working with colleagues in Japan and Germany to propose a laser transponder on the Selene II Lunar Lander Mission [Schreiber et al, 1999], which has been suggested as a possible 2006 follow-on to the Japanese Selene lunar lander mission in 2003.

2. BASIC TRANSPONDER LINK EQUATIONS

The mean number of signal photoelectrons recorded by the terminal B receiver on a single laser fire is given by the transponder link equation [Degnan, 1996; Degnan, 2000a]

$$n_s^B = \frac{C_{AB} E_A A_B}{R^2} \tag{1}$$

where E_A is the pulse energy transmitted from terminal "A" , A_B is the area of the receiving telescope at the receiving terminal "B", R is the distance between the two terminals, C_{AB} is a ***transponder constant*** given by

$$C_{AB} = \frac{\eta_q^B \eta_r^B T_A^{\sec(\theta_A)} T_B^{\sec(\theta_B)}}{h\nu \Omega_t^A}, \tag{2}$$

η_q^B is the detector B quantum efficiency, $h\nu$ is the laser photon energy, T_A and T_B are the one-way zenith atmospheric transmissions at Terminals "A" and "B" (appropriate for two terminals on planetary surfaces), θ_A and θ_B are the local zenith angles for the opposite terminal, Ω_t^A is the transmitter solid angle for laser A,

and η_r^B is the optical throughput efficiency of the receiver B optics respectively. The order of the subscripts in the transponder constant determines the direction of the link, i.e. C_{AB} is the link from terminal A to B. The mean signal at the opposite terminal is obtained by simply interchanging A and B in the above equations.

We can choose to write (1) in terms of the average laser power, i.e.

$$n_s^B = \frac{C_{AB} P_A A_B}{f_{qs} R^2} \tag{3}$$

where f_{qs} is the Q-switching frequency (laser repetition rate) in Hz. We refer to $P_A A_B$ as the ***Mixed Power-Aperture Product*** to reflect the fact that it contains properties of two different terminals. Although not essential, the use of a common laser fire rate in the double-ended transponder link conceptually simplifies the instrument. From (3), the ratio of the mean signal strengths at the two terminals is given by

$$\frac{n_s^B}{n_s^A} = \frac{C_{AB}}{C_{BA}} \frac{P_A A_B}{P_B A_A} \cong \frac{P_A}{A_A} \frac{A_B}{P_B} \tag{4}$$

where, from (1), the approximation holds if the laser beam divergence and detector and optical throughput efficiencies are roughly equal at both ends of the link $(C_{AB} \cong C_{BA})$. Furthermore, the above ratio is approximately unity if the ***Power-to-Aperture Ratio*** is the same at both ends of the transponder link; i.e. $P_A/A_A = P_B/A_B$. We refer to this as a ***balanced*** system [Degnan et al, 1998; Degnan, 2000a]. Note that the signal detection rate is proportional to the Mixed Power-Aperture Product, $P_A A_B$, and that, for a balanced system, the range sampling rate at both terminals is approximately equal. Thus, if it becomes necessary to conserve limited spacecraft resources while still maintaining a balanced link with a fixed sampling rate, one can increase the power and telescope aperture at the Earth station proportionally to maintain the same Power-to- Aperture ratio while simultaneously reducing the transponder laser power and receive aperture at the remote terminal by the same factor.

3.0 NOISE SOURCES

Noise count rates can vary widely depending on whether the transponder is operating (1) in cruise phase between planets, (2) in orbit about the target planet, or (3) from the surface of a "planet" containing a scattering atmosphere. We will use the term "planet" in its broadest sense to include not only the major planets, but also the minor planets (asteroids), moons of major planets, etc. The following three noise sources are present in all of the aforementioned operational scenarios: detector dark counts, solar radiation scattered from the surface and atmosphere of the planet being viewed by the receiver (planetary albedo), and the residual stellar background in the receiver field of view (FOV). The number of counts from the star background within a narrow receiver FOV on the order of 100 μrad (20 arcseconds) are expected to be relatively small compared to those induced by planetary reflections or emissions. Mars under maximum solar illumination, for example, appears as a magnitude -2.5 star when viewed from Earth [Zissis, 1993].

An approximate expression for the noise count rate for the total planetary albedo (Planet A's surface and atmosphere), as viewed by the receiver at Terminal B, is given by [Degnan, 2000a]

$$\dot{n}_{sa}^B \cong \frac{\eta_q^B \eta_r^B}{h\nu} \frac{N_\lambda^A \Delta\lambda_B A_B r_A^2 T_B^{\sec\theta_B}}{R^2} \left[\rho_A g_{ps}^B(\alpha_A) + \frac{1}{2} \ln\left(\frac{1}{T_A}\right) g_{as}(\alpha_A) \right] \tag{5}$$

where N_λ^A is the exoatmospheric solar spectral irradiance at Planet A at the operating wavelength, $\Delta\lambda_B$ is the FWHM bandpass of Terminal B's spectral filter, r_A is the mean volumetric radius of planet A, and ρ_A is the globally averaged surface reflectivity of Planet A. The functions g_{ps}^B and g_{as}^B are geometric factors for the surface and atmospheric contributions, which depend on the fraction of the planetary surface

illuminated by the Sun. The geometric factors fall monotonically from a maximum value of 1 for full solar illumination to 0 for no illumination. The latter can be expressed as a function of the ***aspect angle***, α_A, defined as the angle subtended by two vectors, both originating from Planet A and directed toward the Sun and Planet B respectively as in Figure 1.

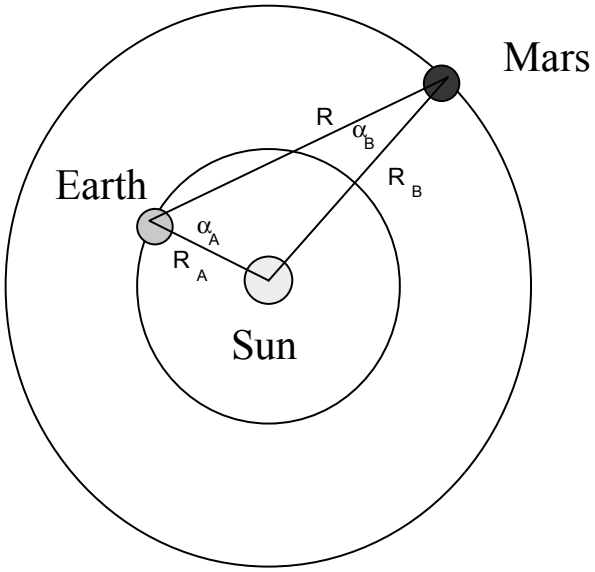

Figure 1: Solar system view of Planets A and B circling the Sun. The aspect angle for Planet A is defined as the angle formed by a vector originating at Planet A and directed toward the Sun and a second vector originating at Planet A and directed toward Planet B other two bodies and vice versa.

For a planetary lander operating in local daylight, we must add the noise background rate caused by solar scattering in the local atmosphere. This is given by the expression [Degnan, 2000a]

$$\dot{n}_{ls}^{B} = \frac{\eta_q^B \eta_r^B}{h\nu} \frac{N_\lambda^B(\Delta\lambda_B) A_B \Omega_r^B}{4\pi} \left\{ \sec\theta_B T_B^{\sec\theta_B} \left[\frac{1 - T_B^{\sec\theta_s - \sec\theta_B}}{\sec\theta_S - \sec\theta_B} \right] \right\} \quad (6)$$

$$\approx \frac{\eta_q^B \eta_r^B}{h\nu} \frac{N_\lambda^B(\Delta\lambda_B) A_B \Omega_r^B}{4\pi} \left\{ T_B^{\sec\theta_B} \ln T_B^{\sec\theta_B} \right\}$$

where Ω_r^B is the receiver field of view in steradians. It should be mentioned that the atmospheric noise model makes no assumptions regarding the distribution of scatterers with altitude. The model does assume no horizontal gradients, however, and therefore depends only on the zenith transmission, T_B, between the station and the "top" of the planetary atmosphere and the local zenith angles of the Sun, θ_S, and of the opposite terminal, θ_B. Note that as $T_B \to 1$ (no scattering), the background count rate due to solar scatter off the atmosphere correctly goes to zero for all values of θ_S and θ_B. The approximation in (6) is independent of θ_S and θ_B and gives generally good results for $\theta_B < 60^o$ for atmospheres with modest to high transmissions ($T_B \geq 0.7$)

During local night operations, the irradiance of the local atmosphere by nearby planetary moons produces background rates that are negligible when compared to planetary albedo. For example, a "full" Moon produces a noise background at the Earth terminal approximately six orders of magnitude less intense than the Sun.

Back-scattered laser radiation produced by the outgoing pulse is an additional time-dependent source of noise and is applicable to both day and night operations from the planetary surface. For a monostatic system (coaxial transmitter and receiver optics), the latter contribution is given by the lidar equation [Degnan, 2000a]

$$\dot{n}_{bs}(\tau) = \frac{\eta_q^B \eta_r^B A_B}{2\pi h\nu} \frac{E_B}{h_{sc}^B c} \left[\ln\left(\frac{1}{T_B}\right) T_B^{2\sec\theta_B\left[1-\exp\left(-\frac{c\tau}{2h_{sc}^B \sec\theta_B}\right)\right]} \right] \left[\frac{e^{-\frac{c\tau}{2h_{sc}^B \sec\theta_B}}}{\tau^2} \right] \tag{7}$$

and falls off rapidly with the time from laser fire, i.e.

$$\tau = \frac{2s}{c} = \frac{2\sec\theta_B}{c}\left(z - h_s^B\right), \tag{8}$$

where s is the distance from the terminal to the scattering volume, h_s^B is the altitude of the station from a nominal reference (e.g. sea level), z is the corresponding altitude of the scattering volume, and h_{sc}^B is the atmospheric scale height. Due to the logarithmic term in (7), the backscatter contribution correctly goes to zero in the absence of a scattering atmosphere. Laser backscatter can be greatly reduced through the use of bistatic optical systems.

At Mars, the Sun is never more than about 41 degrees away from the transponder line-of-sight to Earth. Thus, direct solar illumination of the transponder optics and the resulting scatter within the instrument is another potential source of background noise when the opposite terminal is angularly close to the Sun. System baffling and stray light rejection are therefore important considerations for any practical instrument, but the noise background count rate can be reduced to acceptable levels through the use of solar shields, careful spectral and spatial filtering, and aggressive stray light control.

Compared to other sources of noise, dark count rates in the visible detectors typically used in laser ranging tend to be relatively low (10^2 to 10^4 counts/sec). PhotoMultiplier Tubes (PMT's) typically have far lower dark count rates than Silicon-based Avalanche Photo-Diodes (APD's), but their quantum efficiencies are often significantly lower (15% for PMT vs 50% for APD).

4. ACQUISITION OF THE EARTH TERMINAL

A block diagram of a dual mode Microlaser Altimeter and Transponder (MAT), recently proposed for a mission to the asteroid Vesta, is provided in Figure 2. When in orbit about the planet, the instrument ranges to the surface and provides topographic maps [Degnan, 2000b]. A CCD, boresighted with the range receiver, can provide 2D images of the surface being measured.

The same instrument can function as a transponder at any point within the mission, i.e. during interplanetary cruise phase, in orbit, or from the surface of the planet. In transponder mode, acquisition of the Earth terminal requires an initial search within a three-dimensional volume bounded by the initial angular pointing uncertainty and the uncertainty in the time of arrival of the pulse from the opposite terminal. The latter affects the choice of range gate width and has two components - the uncertainty in the a priori knowledge of range between the two terminals as derived from ephemerides and the uncertainty in the laser fire time at the opposite terminal. Acquisition of the opposite terminal is most easily accomplished in two steps - first in 2-D angular space and then in 1-D range space [Degnan et al, 1998]. The following provides an overview of the acquisition process and key numerical results. For more detail, the reader is referred to [Degnan, 2000a].

The angular search for the Earth terminal is aided by a sensitive CCD array capable of imaging the Earth, Moon, and nearby stars within a nominal 1^o x 1^o degree field of angular uncertainty. For a transponder

mounted to the spacecraft body, this level of angular uncertainty is inclusive of the error associated with the pointing of a spacecraft from orbit or during interplanetary cruise phase. It is also inclusive of the expected angular error in the case where the transponder is assumed mounted to a meter-class K-band microwave communications dish communicating with Earth. Using pointing corrections to an independent two-axis transponder gimbal mount of limited angular range ($<2^o$), or alternatively a pair of Image Motion Compensators (IMC's) [McElroy et al, 1977], to implement the fine pointing of the receiver, the system computer can center and hold the Earth image in the CCD array. Space-qualified, high sensitivity CCD cameras with up to 2048 x 2048 pixel resolution are readily available and yield a 8.8 μrad single pixel resolution for a nominal 1^ox1^o array FOV. Since the full Earth disk subtends an angular width between 34 and 163 μrad (i.e. 4 to 19 pixels across) from Mars at its farthest and closest points from Earth respectively, the center of the Earth image can be well resolved at the sub-arcsecond level. In planetary orbit or during cruise phase, the transponder CCD sees a rather bright sunlit Earth against a dark background. Even when the Earth's "nightside" is largely directed toward the transponder, there can be sufficient forward scattering of solar light by the Earth's atmospheric rim for detection [Mallama, 1998].

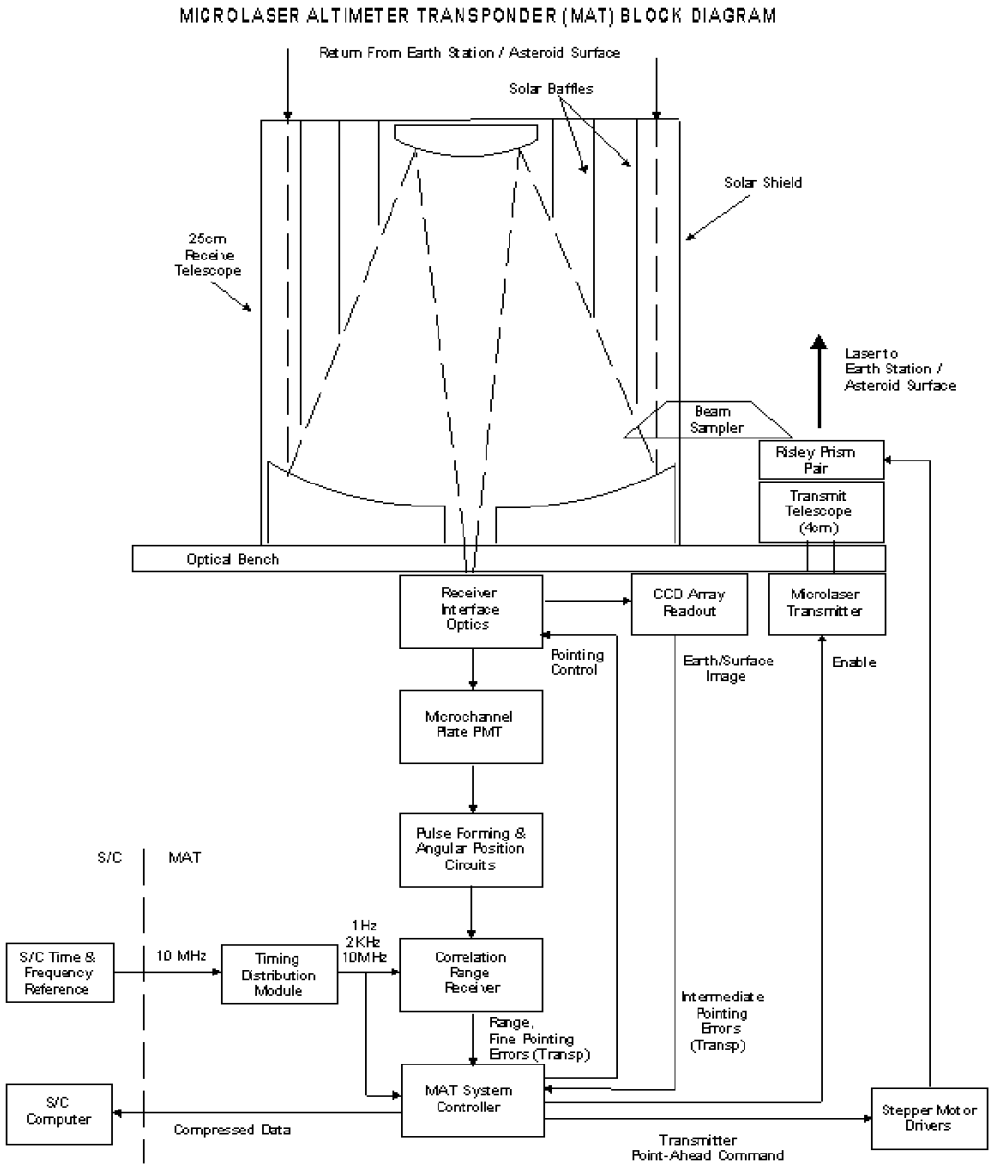

Figure 2: Block diagram of a dual-mode Microlaser Altimeter Transponder (MAT) instrument.

The worst case noise scenario is for a transponder on the planet's surface operating in local daylight in the presence of a scattering atmosphere. Fortunately, the resulting background count rate is distributed over all of the pixels of the CCD whereas the solar radiation scattered from the opposite planet is distributed only over a subset of pixels. Using (5) and (6), an approximate expression for the CCD contrast of the planetary image at terminal B is [Degnan, 2000a]

$$C_{CCD}^{B} \approx 1 + \frac{4}{f_A}\left(\frac{R_B}{R_A}\right)^2 \frac{\left[\rho_A g_{ps}^{B}(\alpha_A) + \frac{1}{2}\ln\left(\frac{1}{T_A}\right) g_{as}^{B}(\alpha_A)\right]}{\ln\left(\frac{1}{T_B^{\sec\theta_B}}\right)} \tag{9}$$

where R_A and R_B are the mean orbital radii for planets A and B, and f_A is the fraction of Planet A's disk illuminated by the Sun as seen from Planet B. Figure 3 plots the contrast of the Mars, Earth, and Moon images against the scattering of solar radiation by the local atmosphere during daylight operations as a function of the synodic phase.

Once the Earth is centered in the receiver FOV, receipt of laser pulses from Earth is ensured provided: (1) the Earth ground station pointing error is less than the ground laser beam divergence (nominally about 50 μrad); (2) the range receiver FOV is larger than the Earth disk and is adequately boresighted with the CCD array; and (3) there is sufficient signal to surpass the detection threshold of the receiver. Angular errors due to uncertainties in planetary and most other ephemerides to important bodies in the inner Solar System are typically far smaller (< 0.01 μrad) than the nominal laser beam divergence assumed here (50 μrad) as are the pointing control errors in a star-calibrated, meter-class telescope/tracking system (<15 μrad). Furthermore, arriving laser photons can be detected by a quadrant ranging detector, which is co-aligned with the center of the CCD array. As in NASA's developmental SLR2000 satellite laser ranging station, the quadrant detector permits fine pointing corrections of the transponder receiver at the subarcsecond level [Degnan and McGarry, 1997].

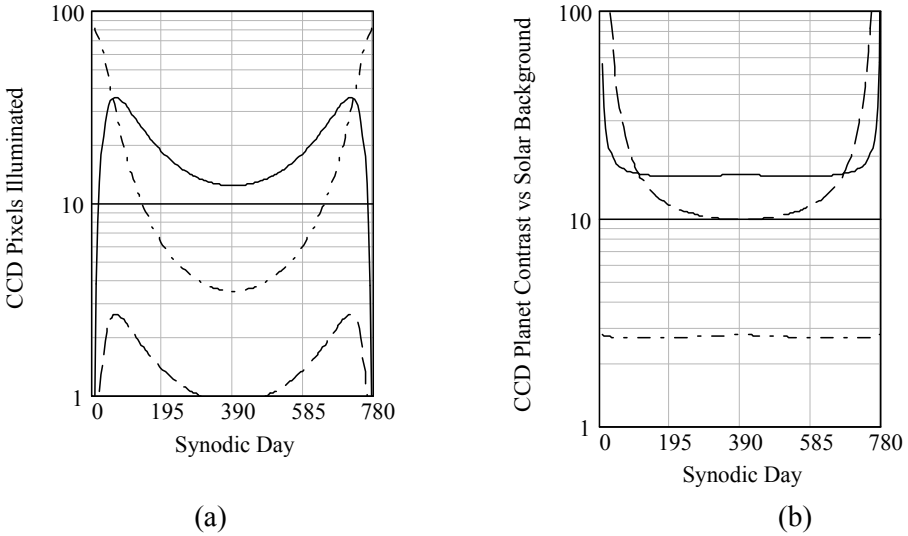

Figure 3: (a) Number of CCD pixels illuminated by the Earth (solid), Mars (dot-dash), and Moon (dash) images; (b) Contrast of image to background counts caused by solar scattering from the local atmosphere during daylight operations. Assumes 2048x2048 pixel array monitoring 1^ox1^o FOV.

Once the CCD image determines where the Earth was situated one transit time ago, a point-ahead correction must be applied to the transmitted beam via a pair of Risley prisms. The magnitude of the point ahead can be calculated from onboard orbital models for the two planets whereas the direction of Earth's forward motion is given by the placement of other bodies, such as the Moon or stars, within the CCD field of view [Degnan et al, 1998; Degnan, 2000a]. Verification of transmitter pointing can be obtained by reflecting a fraction of the outgoing laser beam into the receiver as in Figure 2.

To simplify the discussion of acquisition in range space, we will assume that the two transponders have a common laser fire interval, τ_{qs}. During each interval or cycle, each terminal records the time of departure of the outgoing pulse and the time of arrival of any incoming pulses relative to a fixed sub-clock, which is counting at the nominal laser fire rate and is derived from a highly accurate frequency standard such as a rubidium or cesium clock. In the case of a Mars lander, an onboard knowledge of the Earth and Mars ephemerides and planetary spin axis orientation and rotation rates permits a fair a priori estimate of the interplanetary distance (typically within a few tens of kilometers), the differential pointing angle (within an arcsecond), and the forward direction of the Earth's motion. If the distance between terminals can be known a priori to well within the distance light travels in one laser fire interval, the incoming pulse can be easily matched up with the proper cycle at the opposite terminal where it originated. Because light transit times within the inner Solar System can span several tens of minutes, there may be thousands to millions of cycles between the matching cycles for each terminal, depending on the laser fire rate and interplanetary distance. During initial acquisition, the initial uncertainty in the laser time of fire at the opposite terminal can be as large as the laser fire interval itself if the clocks at Terminals A and B have not been compared in some time and are totally uncorrelated. Once a successful two-way link is established, however, this uncertainty shrinks rapidly, allowing the receivers to be gated over a much narrower time interval.

Every range receiver is characterized by a ***range gate***, a ***range bin***, and a ***detection threshold***. In a single-ended range measurement to a passive reflector, the ***range gate***, τ_g, provides a temporal filter for the reduction of background noise and is chosen large enough to encompass the uncertainty in our a priori knowledge of the range to the target. The ***range bin***, τ_b, is the time over which the receiver integrates the incoming signal and is optimally chosen, in conventional high SNR systems, to be just large enough to capture the majority of the signal photons within a single pulse. In the case of photon-counting receivers [Degnan, 2000b], a somewhat larger range bin is chosen to collect the photons from a collection of multiple pulses over a time interval referred to as a ***frame***. In either case, the number of range bins within the range gate is given by the simple formula

$$N_{bin} = \frac{\tau_g}{\tau_b} \tag{10}$$

We refer to the 2D areas defined by the horizontal borders of the "range bins" and the vertical borders of the "frames" as ***cells***. A consecutive sequence of frames is a ***super-frame*** [Degnan, 2000b]. We tentatively identify potential ***signal cells*** within a given frame by counting all of the photoelectrons generated within each cell and comparing it to a ***frame threshold***. We refer to this basic data processing scheme, which was used in LLR data processing [Abbott, et al, 1973], as ***Post-Detection Poisson Filtering***.

In a satellite laser ranging system, the range between ground station and satellite changes rapidly and the position of the range gate is varied in real time, based on an a priori range estimate, in an attempt to keep the satellite return centered in the gate. The measured pulse times of flight, displayed on the ordinate axis relative to the center of the range gate versus elapsed time on the abscissa, is referred to as an Observed Minus Calculated (O-C) plot [Degnan, 1985]. If our a priori range and range rate corrections and satellite force models were perfect and additionally there were no range or time biases in the computed orbit, the corresponding "Observed Minus Calculated" (O-C) curve would place all of the observed signal photons within a single range bin centered in the range gate. In this highly idealized example, the temporal width of the signal data distribution would then be determined by the timing precision of the range receiver and small atmosphere-induced fluctuations which, in modern SLR systems, is characterized by a one sigma RMS single-shot range scatter of one cm (67 picoseconds) or less [Degnan, 1993]. Background photons and detector dark counts, on the other hand, are randomly distributed throughout the entire range gate.

Thus, when histogrammed into individual range bins, the signal counts stand out from the background due to their high "temporal" correlation in the range axis [Degnan, 2000a].

In real SLR systems, range biases displace the signal from the center of the range window, and orbital time biases introduce a slope in the signal data as viewed in an O-C plot. Once a slope is observed in the data, however, a time bias correction can be iteratively applied in the range model as necessary to reduce the slope and ultimately the size of the range bin and/or gate for better signal contrast and noise rejection. A similar phenomenon will occur in an asynchronous transponder link when a range-rate, estimated from planetary ephemerides and applied to the photon arrival times, has a residual error. Interplanetary range rates can be quite high, on the order of 55 km/sec for the Earth-Mars link. Fortunately, the error in range rate, as computed from contemporary ephemerides for Earth and Mars, is estimated to be less than 1 cm/sec [Lemoine, 2000]. This corresponds to a slope of less than 33 psec/sec in the O-C curve after the computed range rate is subtracted from the raw range data. A second component of range rate resulting from rotation of station A about its planetary axis is a sinusoidal function with peak amplitude

$$\left|\dot{r}_A\right|_{\max} = \varpi_A r_A \cos\lambda_A \cos i_A \tag{11}$$

where ϖ_A is the angular rotation rate about the spin axis, r_A is the volumetric mean radius of Planet A, λ_A is the latitude of the station, and i_A is the inclination of the spin axis to the orbital plane. An identical expression applies to the station on Planet B. Using the constants in Table 1, the maximum range rate introduced by the rotation of Earth and Mars for equatorial stations is 67.6 m/sec and 34.6 m/sec respectively and decreases with increasing latitude. Thus, (10) predicts O-C slopes between 0 (for polar stations) and 230 nsec/sec (for equatorial stations) due to Earth rotation and between 0 and 120 nsec/sec due to Mars rotation. The maximum values are large enough to suggest that an a priori correction for planetary rotation be applied to the data prior to producing the O-C plot in order to further sharpen the resulting histogram peak and improve the signal contrast.

PLANETARY PARAMETER	EARTH (A)	MARS(B)	MOON (A')
Mean Distance from Sun, R (AU ~ 150 x 10^6 km)	1.0	1.52	1.0
Length of Year, τ(Earth days)	365.256	686.98	NA
Length of day, hours	24	24.657	NA
Obliquity of Spin Axis to Orbital plane, deg	23.45	25.19	NA
Mean Volumetric Radius, km	6371	3390	1738
Mean Surface Reflectivity @ 532 nm, ρ	0.15 (est.)	0.15 (est)	0.12
Atmospheric Transmission @532 nm, T	0.7	0.9 (est)	1.0

Table 1: Planetary parameters assumed in the link calculations.

Double-ended transponder systems use two clocks and two lasers whereas a single-ended SLR system uses only one laser and one clock in recording the pulse time of flight, and this difference leads to some additional range errors as recorded in a transponder O-C plot. For example, if the frequency standards (clocks) at the two interacting transponder terminals have a frequency offset, there will be an additional contribution to the observed slope given by the familiar Doppler equation, i.e.

$$\sigma_c = -c\frac{\Delta f}{f_c} \tag{12}$$

where f_c is the nominal clock frequency at both terminals and Δf is the offset frequency between the clocks. A fractional clock offset less than 1 x 10^{-11} (easily achieved by a rubidium or cesium standard) corresponds to a range rate error less than 3 mm/sec, or about 20 psec/sec, which is comparable in magnitude to the a priori range-rate error from the ephemerides. For an undisciplined quartz crystal oscillator, however, the slope could be up to two orders of magnitude higher.

A further difference arises from the use of two lasers. In a single-ended SLR system, the RMS scatter of the data depends on the jitter in the detector response, the resolution of the timer, and the impulse response of the satellite. Any jitter in the laser fire time cancels out of the range measurements since the start and stop pulses input to the interval timer are affected equally. However, in a two-way asynchronous transponder, the unequal and uncorrelated jitter in the fire times of the two lasers leads to an additional random range error, which would be expected to dominate the overall jitter contribution and broaden the signal data in the O-C plot relative to the single laser case.

Any slope or breadth to the signal data must be accommodated by our choice of range bin. The breadth or precision of the signal data sets a lower limit on the range bin size, even for automated high SNR single pulse detection. With a residual data slope, any increase in the receiver integration (frame) time in a low SNR photon-counting system must be accompanied by a proportional increase in the range bin width to ensure that we capture all of the signal photons from multiple laser fires in a single cell. One rule of thumb that appears to work well in our simulations is to choose a bin size at least twice as large as the expected overall RMS variation in the O-C range data over a frame, i.e.

$$\tau_b \geq 2\sqrt{\left(\left\langle \sigma_e^{\,2} \right\rangle + \left\langle \sigma_r^{\,2} \right\rangle + \left\langle \sigma_c^{\,2} \right\rangle\right)\tau_F^2 + \left\langle \tau_A^2 \right\rangle + \left\langle \tau_B^2 \right\rangle} \tag{13}$$

where $<\sigma_e^2>$, $<\sigma_r^2>$, and $<\sigma_c^2>$ are the expected variances in the residual slopes in O-C space due to errors in ephemerides, planetary rotation rates, and clock offsets respectively, τ_F is the frame time, and $<\tau_A^2>$ and $<\tau_B^2>$ are the variances in the recorded fire times (including laser, detector and timer jitter) at terminals A and B respectively.

The ***detection threshold*, *K*,** is used to determine the probable presence of signal against a noise background. For single pulse detection in a high SNR system, the threshold is usually set by hardware whereas, for low SNR photon-counting systems, the threshold is usually set by a combination of hardware (e.g. a range receiver or multichannel scalar) and software which compares the counts in each bin/cell to a ***frame threshold, K,*** and rejects counts below the threshold as probable noise [Degnan, 2000b]. In either case, choosing too high a threshold results in the loss of valid range returns, whereas choosing too low a threshold results in increased noise-induced false alarms. Furthermore, because of the potentially large number of cells in a frame (especially during acquisition when range uncertainties are largest), it is possible that a sizable number of noise cells in a given frame will be falsely identified as signal even when the probability of false alarm for any given noise cell is relatively small. One approach to optimizing the frame threshold is to maximize the ***Differential Cell Count*** [Degnan, 2000b], defined as the mean number of correctly identified signal cells minus the mean number of false alarms in cells containing only solar background counts within a ***superframe*** consisting of M frames, i.e.

$$\delta N = M\left[P_d^B - N_{bin}P_{fa}^B\right] \tag{14}$$

where P_d^B is the probability of correctly identifying the signal cell within a frame and P_{fa}^B is the probability of falsely identifying a noise cell as signal. This approach yields an "optimum" threshold condition for Terminal B given by [Degnan, 2000b]

$$K_{opt}^B = \frac{N_s^B + \ln(N_{bin})}{\ln C_B} = \frac{(C_B - 1)N_b^B + \ln(N_{bin})}{\ln C_B} \tag{15}$$

where N_{bin} is the number of range bins defined by (10), N_s^B is the mean signal count in the signal cell, N_b^B is the mean noise count in any given cell, and $C_B = 1 + N_s^B / N_b^B$ is the ***signal cell contrast*** at Terminal B. From Poisson statistics, the probability of correctly detecting the signal cell is given by

$$P_d^B = e^{-C_B N_b^B} \sum_{k=K_{opt}}^{\infty} \frac{\left(C_B N_b^B\right)^k}{k!} \approx \frac{1}{\sqrt{2\pi C_B N_b^B}} \int_{K_{opt}}^{\infty} dN \exp\left[-\frac{(N - C_B N_b^B)^2}{2 C_B N_b^B}\right] = \frac{1}{2}\left[1 + erf\left(\frac{C_B N_b^B - K_{opt}^B}{\sqrt{2 C_B N_b^B}}\right)\right] \tag{16}$$

where, in the limit of "large" mean counts (>15), one can use the Central Limit Theorem to approximate the Poisson distribution by a Gaussian (normal) distribution and erf(x) is the familiar ***error function***. Similarly, the probability of false alarm is given by

$$P_{fa}^B = e^{-N_b^B} \sum_{k=K_{opt}}^{\infty} \frac{\left(N_b^B\right)^k}{k!} \approx \frac{1}{\sqrt{2\pi N_b^B}} \int_{K_{opt}}^{\infty} dN \exp\left[-\frac{(N - N_b^B)^2}{2 N_b^B}\right] = \frac{1}{2}\left[1 - erf\left(\frac{K_{opt}^B - N_b^B}{\sqrt{2 N_b^B}}\right)\right] \tag{17}$$

The error function expressions can be used in the usual case where the optimum threshold lies between the peaks of the noise and signal cell populations, i.e. if we satisfy the condition $N_b^B < K_{opt} < C_B N_b^B = N_s^B + N_b^B$.

For weaker signals, a powerful second test can be applied, if necessary, by requiring that cells in adjoining frames be ***correlated***. In the most general sense, this simply means that cells tentatively identified as containing "signal" in adjacent frames must obey applicable physical laws or constraints. For example, the physical laws governing planetary or spacecraft motion do not allow the transponder position to make unexpected discontinuous jumps into widely separated range bins between frames. Thus, we can define a "valid trajectory" as one where the planet or spacecraft position changes by no more than one range bin in moving between frames and monotonically moves in the correct direction on either side of the range extrema. This correlation requirement allows us to apply an "N of M" test on multiple cells which survive the initial threshold test within a ***superframe*** and recover missing signal cells . For signal verification, the "N of M" test requires that at least N cells, all satisfying the threshold criteria and lying on a valid trajectory, be detected within the M successive frames comprising the superframe. Based on successful application of this test, any signal data in the up to (M-N) signal cells, which may have originally failed to meet the threshold criteria, can be successfully restored via interpolation between frames [Titterton et al, 1998; Degnan, 2000b].

5. HIGH SNR LINK: MOBLAS TO "GREEN MOLA"

Our first link example will be a conventional high Signal-to-Noise Ratio (SNR) link between a NASA Mobile Laser (MOBLAS) station [Degnan, 1985] and a 532 nm (green), subnanosecond version of the Mars Orbiter Laser Altimeter (MOLA) instrument [Smith et al, 1999], both of which are operating at a zenith angle of 30^o. The laser energy of the "green MOLA" was chosen to provide a balanced transponder link with MOBLAS assuming the 50 cm MOLA receive aperture. Coincidentally, the green pulse energy of 43 mJ, multiplied by the MOBLAS repetition rate of 5 Hz yields an average power of 215 mW which is roughly half the 1064 nm power produced by the MOLA instrument at 10 Hz. Thus, the reduction in repetition rate compensates for the roughly 50% loss in laser power due to conversion of the fundamental Nd:YAG wavelength from 1064 nm to 532 nm so that the "green MOLA" should consume roughly the same prime power as the original MOLA. In both systems, we assume an improved transmitter beam divergence of 50 μrad with a somewhat wider receiver FOV of 100 μrad in order to accommodate residual boresight errors/drifts between the transmitter and receiver. Table 2 summarizes the assumed instrumental parameters for the high SNR link.

In this high SNR example, we assume that each terminal detects single subnanosecond pulses, i.e. one laser fire per cell. We therefore select a range bin size, τ_b = 1 nsec, which comfortably accomodates all of the signal photons in a single pulse. We further assume the worst case scenario of totally unsynchronized

clocks at Terminals A and B so that the receiver is initially ungated for the entire interpulse period of 200 msec. This results in a very large number of range bins, i.e. $N_{bin} = 2 \times 10^8$. In Figure 4, we plot: (a) the optimum threshold; (b) the differential cell count; (c) the probability of correctly detecting the signal cell; and (d) the mean false alarms per laser fire for the Earth and Mars terminals as a function of the synodic phase for both night and day operations.

Parameter	MOBLAS (A)	"Green MOLA" (B)
Transmitted Pulse Energy, mJ	100	43
Repetition Rate, Hz	5	5
Average Power @532 nm, mW	500	215
FWHM Pulsewidth, psec	150	<1000
FWHM Beam Divergence, μrad	50	50
Telescope Diameter, cm	76	50
Detector Quantum Efficiency, %	12	12
Receiver Throughput, %	40	40
Receiver FOV, μrad	100	100
FWHM Spectral Filter, nm	0.3	0.3
Range Gate, msec (ungated)	200	200
Range Bin, nsec	1	1
Spacecraft Zenith Angle, deg	30	30

Table 2: Instrumental parameters assumed in the link calculations for a conventional high SNR balanced transponder pair operating between Earth and Mars.

During the first quarter of the synodic cycle, the optimum threshold drops from roughly 15-18 pe to 3-4 pe then levels off for two quarter cycles before climbing again to the 15-18 pe level during the last quarter. Near minimum interplanetary range, the signal is higher and the optimum threshold tends to higher values so that the differential cell count algorithm can suppress the number of false alarms to a negligible number without significantly affecting the signal detection probability. Near maximum range, the algorithm lowers the threshold to allow a higher probability of detection for the weaker signal but in the process makes false alarms more likely. The probability of successfully detecting the signal is essentially unity for the first and last quarter cycle for both terminals under both day and night conditions. A negligible number of false alarms occur (<1 per fire) under both day and night scenarios during the first and last quarters. Even near the point of maximum interplanetary range, the detection probability for daylight operations drops to about 86% for the Earth terminal and 90% for the Mars terminal. Furthermore, because of the lowered threshold near the point of maximum range and the huge number of 1 nsec range bins within the ungated laser fire period of 200 msec, the mean false alarms can jump to about 1 in 1000 frames at Earth and to about 1 in 15 frames at Mars in spite of an extremely low false alarm probability per bin which is on the order of 5×10^{-8} for the Earth terminal and 5×10^{-7} for the Mars terminal. Nevertheless, the false alarms are widely scattered throughout the laser fire interval whereas the 5 Hz signal counts will stand out prominently against the false counts when displayed in a histogrammed O-C plot because of their temporal coherence. Furthermore, once the signal is acquired, the range gate can be narrowed sufficiently to suppress virtually all subsequent false alarms.

6. LOW SNR LINK: SLR2000 RANGING TO A "GREEN MLA"

We now provide an example of a low SNR link where multiple single photon returns in a high repetition rate link are accumulated in the cells of a correlation range receiver. The potential advantages of such a system have been described previously [Degnan et al, 1998; Degnan, 2000a]. The Earth ground station is assumed to be NASA's developmental SLR2000 station [Degnan and McGarry, 1997] and the Mars terminal is assumed to be similar in size to the Messenger Mercury Laser Altimeter (MLA), which is smaller and more lightweight than the Mars MOLA instrument. Both instruments are assumed to use compact, low energy, microlaser transmitters which operate at a much higher 2 kHz rate [Degnan and Zayhowski, 1998]. The laser energy of the "green MLA" was again chosen to provide a balanced

transponder link with SLR2000 assuming the 25 cm MLA receive aperture. The instrument characteristics are summarized in Table 3.

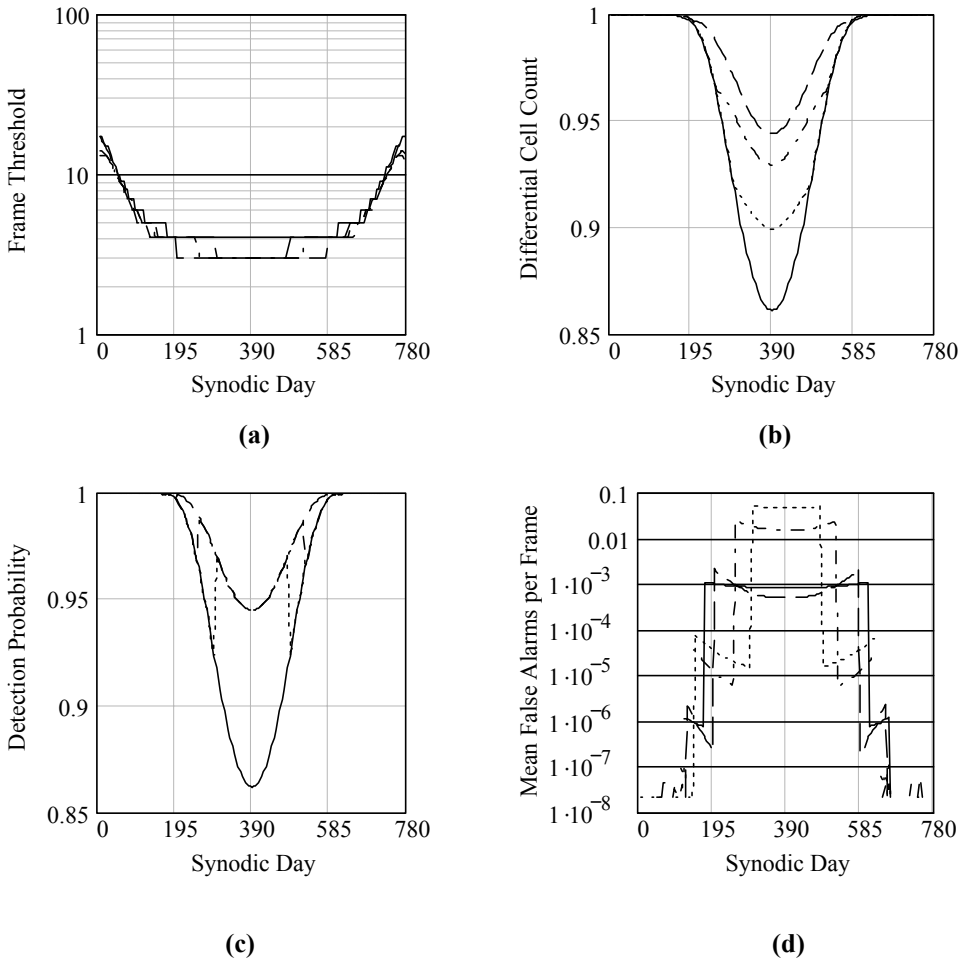

Figure 4: Operating parameters as a function of synodic phase/day for the balanced, high SNR Earth-Mars transponder link operating at 5 Hz during initial acquisition under worst case conditions of unsynchronized clocks: (a) optimum detection threshold; (b) optimized differential cell count; (c) optimized signal detection probability; and (d) mean false alarms per laser fire. Earth daylight and night operations are indicated by the solid and dashed lines respectively; Mars daylight and night operations are represented by dotted and dash-dotted lines respectively.

In this low SNR example, we select a range bin size, τ_b = 2 nsec, which comfortably accomodates all of the signal photons. We again assume the worst case scenario of totally unsynchronized clocks at Terminals A and B so that the receiver is initially ungated for the entire interpulse period of 0.5 msec, but the higher repetition rate results in a much smaller number of range bins, i.e. N_{bin} = 2.5 x 10^5. We plot, in Figure 5: (a) the optimum threshold; (b) the differential cell count; (c) the probability of detecting the signal cell; (d) the mean false alarms per laser fire; and (e) the number of interplanetary range measurements per second for the Earth and Mars terminals as a function of the synodic day for both night and day operations. Because we have assumed a "balanced" system, the frequency of recorded ranges is the same at both terminals.

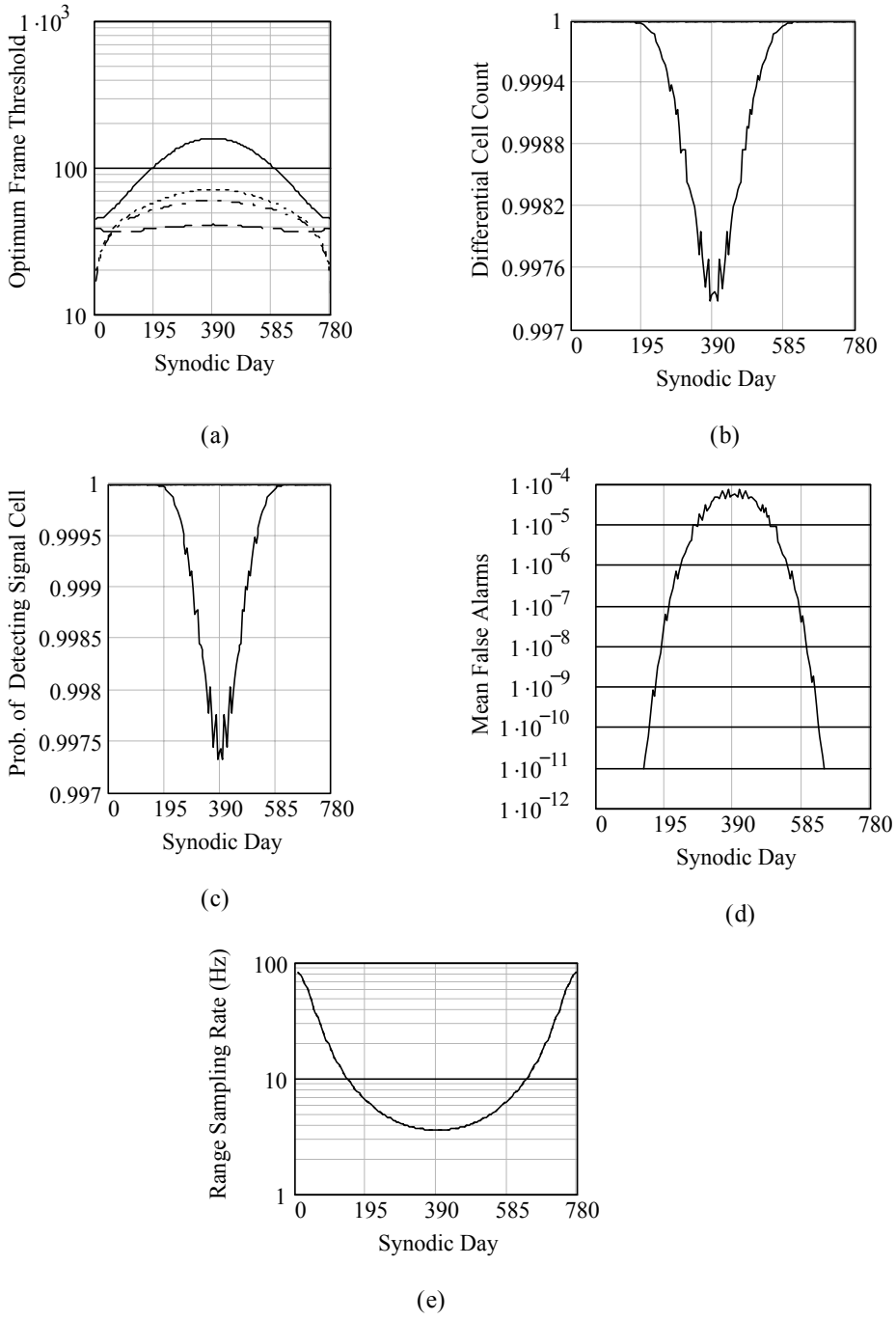

Figure 5: Operating parameters as a function of synodic phase/day for the balanced, low SNR, photon-counting Earth-Mars transponder link operating at 2 kHz during initial acquisition under worst case conditions of unsynchronized clocks: (a) optimum detection threshold; (b) optimized differential cell count; (c) optimized signal detection probability; (d) mean false alarms per laser fire; and (e) range sampling rate (same at both terminals since they are "balanced"). Earth daylight and night operations are indicated by the solid and dashed lines respectively; Mars daylight and night operations are represented by dotted and dash-dotted lines respectively.

The behavior of the high and low SNR links as a function of synodic phase are both qualitatively and quantitatively different. Instead of decreasing during the first quarter of the synodic cycle and leveling off as in the high SNR case, the optimum frame threshold in the photon-counting example climbs, under local daylight conditions, from roughly 10 pe to perhaps 70 pe for the Mars terminal and from 45 pe to 170 pe for the Earth terminal at maximum interplanetary range and then falls off symmetrically during the second half of the synodic cycle. This behavior occurs because, at longer interplanetary ranges, it takes longer to collect the signal photons necessary to unambiguously distinguish the signal cell from the noise cells. The longer frame time results in a higher mean noise count per cell, which in turn drives the optimum frame threshold higher. The effectiveness of our optimum threshold algorithm is demonstrated by the fact that the Normalized Differential Cell Count, with a maximum value of 1, never drops below 0.997 at either terminal during either day or night operations. Similarly, the probability of correctly identifying the signal cell is greater than 99.7% under all conditions, and the mean false alarm rate is less than one cell in 10,000 frames under the worst case condition of unsynchronized clocks. As in the high SNR case, the number of false alarms is driven down further once the opposite terminal is acquired and the range gate shrunk accordingly. We also note that the rate of range returns at maximum range is 4 Hz, only slightly lower than the nearly fixed 5 Hz rate of the high SNR case, but rises to approximately 80 Hz near minimum range. It should be further noted that the Mixed Power-Aperture Product for this low SNR example is 0.013 Watt-m^2 or 7.5 times smaller than the same product in the high SNR case (.098 Watt-m^2). Thus, even with a smaller Mixed Power-Aperture Product, a significantly higher range sampling rate can be obtained with the low SNR photon-counting system over the full synodic period.

Parameter	**SLR2000(A)**	**"Green MLA" (B)**
Transmitted Pulse Energy, mJ	0.130	0.053
Repetition Rate, Hz	2000	2000
Average Laser Power, mW	260	103
FWHM Pulsewidth, psec	200	<1000
FWHM Beam Divergence, μrad	50	50
Telescope Diameter, cm	40	25
Detector Quantum Efficiency, %	12%	12%
Receiver Optical Efficiency, %	40	40
Receiver FOV, μrad	100	100
Spectral Bandwidth, nm	0.3	0.3
Range Gate, msec (ungated)	0.5	0.5
Range Bin, nsec	2	2
Spacecraft Zenith Angle, deg	30	30

Table 3: Instrumental parameters assumed in the link calculations for a balanced, low SNR (photon-counting) transponder pair operating between Earth and Mars.

7. SUMMARY

An Earth-Mars transponder link is within the SLR state-of-the-art. A MOBLAS station is capable of ranging to a "green MOLA" over the full range of interplanetary distances at a 5 Hz rate using a conventional high SNR approach. The automated SLR2000 system could range to a smaller Messenger-sized transponder in photon-counting mode at a sampling rate of 4 to 80 Hz, depending on the interplanetary range. Analysis indicates that both transponders would be capable of operating from the planetary surface under local daylight conditions.

Signal acquisition of the opposite terminal can be accomplished in a two stage process under both local day and night conditions in the presence of a scattering atmosphere. The partially illuminated planetary disk has sufficient contrast against the local solar background to be seen in the CCD for the initial angular acquisition. Signal acquisition in the third dimension, or range, is simplified by the fact that the range rate can be predicted with an accuracy better than 1 cm/sec. Nevertheless, wide range gates are required during initial acquisition due to the following:

- A priori uncertainties in Earth-Mars range may be as large as 60 km based on comparison of recent generation JPL ephemerides
- There is uncertainty in the time of laser fire at the opposite terminal due to lack of synchronization in the two clocks as well as laser pulse jitter within the clock cycle whereas pulse jitter cancels out in single-ended SLR systems.
- The worst case uncertainty is equal to the laser fire interval in the case of totally unsynchronized clocks and ungated operation.

However, the range gate can be narrowed and the performance improved via lowered thresholds following acquisition.

Finally, the transponder accuracy is greatly improved and operational analysis simplified if a high quality spaceborne clock (e.g. rubidium or cesium) is used. With a high quality atomic clock onboard, decimeter ranging and subnanosecond time transfers should be readily achievable. Further investigations are warranted to determine whether or not the spaceborne clock can be sufficiently "disciplined" by an Earth-based maser, via the time transfer process, to achieve centimeter or even millimeter level ranging between the planets.

REFERENCES

Abbott, R. I., Shelus, P. J., Mulholland, R., Silverberg, E., 1973, Laser Observations of the Moon: Identification and Construction of Normal Points for 1969-1971, The Astronomical Journal, 78, pp. 784-793.

Bender, P. L., Faller, J. E., Hall, J. L., Degnan, J. J., Dickey, J. O., Newhall, X.X., Williams, J. G., King, R. W., Machnik, L. O., O'Gara, D., Ricklefs, R. L., Shelus, P. J., Whipple, A. L., Wiant, J. R., Veillet, C., 1990, Microwave and Optical Lunar Transponders, in Astrophysics from the Moon, AIP Conf. Proc. Series, (American Institute of Physics New York) April.

Degnan, J. J., 1985, Satellite Laser Ranging: Current Status and Future Prospects, IEEE Transactions on Geoscience and Remote Sensing, GE-23, pp. 398-413.

Degnan, J. J., 1993, Millimeter Accuracy Satellite Laser Ranging: A Review, Contributions of Space Geodynamics: Technology, D. E. Smith and D. L. Turcotte (Eds.), AGU Geodynamics Series, Volume 25, pp. 133-162.

Degnan, J. J., 1996, Compact laser transponders for interplanetary ranging and time transfer, Proc. 10th International Workshop on Laser Ranging, pp. 24-31, Shanghai, China, November 11-15.

Degnan, J. J., 2000a, Asynchronous laser transponders for precise interplanetary ranging and time transfer, submitted to J. Geodynamics.

Degnan, J. J., 2000b, Photon-counting multikilohertz microlaser altimeters for airborne and spaceborne topographic measurements, submitted to J. Geodynamics.

Degnan, J. J., McGarry, J. F., 1997, SLR2000: Eyesafe and autonomous single photoelectron satellite laser ranging at kilohertz rates, SPIE Proceedings Volume 3218, Laser Radar Ranging and Atmospheric Lidar Techniques, pp. 63-77, London, UK, September 24-27.

Degnan, J.J, McGarry, J., Dabney, P., Zagwodzki, T., Tierney, M., Weatherley, M., 1998, Design and Test of a Breadboard Interplanetary Laser Transponder, Proc. 11th International Workshop on Laser Ranging, pp. 716-728, Deggendorf, Germany, Sept. 21-25.

Degnan, J.J., Zayhowski, J.J., 1998, SLR2000 Microlaser Performance: Theory vs Experiment, Proc. 11th International Workshop on Laser Ranging, Vol. 2, pp. 458-468, Deggendorf, Germany, Sept. 21-25, 1998.

Lemoine, F. J., 2000, NASA Goddard Space Flight Center, Greenbelt, MD 20771, USA, private communication.

Mallama A., 1998, Earth as seen from Vesta for the transponder proposal, Raytheon STX Corporation Memo to NASA Goddard Space Flight Center, Greenbelt, MD 20771 USA, May 13.

McElroy, J. H., McAvoy, N., Johnson, E. H., Degnan, J. J., Goodwin, F. E., Henderson, D. M., Nussmeier, T. A., Stokes, L. S., Peyton, B. J., Flattau, T., 1977, CO_2 Laser Communication Systems for Near Earth Space Applications, Proc. IEEE, 65, pp. 221-251.

Schreiber, U., Kawano, N., Yoshino, T., Degnan, J., Nordtvedt, K., Muller, J., Schluter, W. and Kunimori, H., 1999, Proc. International Workshop on GEodetic Measurements by the collocation of Space Techniques ON Earth (GEMSTONE), pp. 131-136, Communications Research Laboratory, Koganei, Tokyo, Japan, January 25-28.

Smith, D.E., Zuber, M.T., Solomon, S.C., Phillips, R.J., Head, J.W., Garvin, J.B., Banerdt, W.B., Muhleman, D.O., Pettengill, G.H., Neumann, G.A., Lemoine, F.G., Abshire, J.B., Aharonson, O., Brown, C.D., Hauck, S.A., Ivanov, A.B., McGovern, P.J., Zwally, H.J., Duxbury, T.C., 1999, The global topography of Mars and implications for surface evolution, Science, 284, pp. 1495-1503.

Titterton, P. ,Sweeney, H., Leonard, D., 1998, System/usage impact of operating the SLR2000 at 2 kHz, Proc. 11th International Workshop on Laser Ranging, Deggendorf, Germany, pp.426-437, September 21-25

Zissis, G. J. (ed.), The Infrared and Electro-optical Systems Handbook, Volume 1: Sources of Radiation, Chapter 3, SPIE Optical Engineering Press, Bellingham, WA, USA, 1993.